ACS Photonics
pubs.acs.org/journal/apchd5
Article

A GaAs/AlGaAs LED with SI-GaAs Substrate for X-ray Detection and Imaging: A Down-Conversion Method

Quan Yu, Fangbao Wang, Xin Yuan, Ying Liu, Lianghua Gan, Gangyi Xu, Wenzhong Shen,* Liang Chen,* and Yueheng Zhang*

Cite This: ACS Photonics 2025, 12, 6028−6036

Read Online

ACCESS | Metrics & More | Article Recommendations | Supporting Information

Downloaded via SHANGHAI JIAO TONG UNIV on February 2, 2026 at 02:59:18 (UTC).
See https://pubs.acs.org/sharingguidelines for options on how to legitimately share published articles.

ABSTRACT: GaAs-based light-emitting diodes (LEDs) are commonly employed in a variety of applications, including medical imaging, biosensing, optical communications, and night vision. In this paper, we present an alternative application of a GaAs-based LED with a semi-insulating GaAs (SI-GaAs) substrate for X-ray detection and imaging. The mechanism relies on the semiconductor frequency down-conversion process, where the SI-GaAs substrate acts as a photodetector (PD). Upon X-ray irradiation, the photocurrent generated by the SI-GaAs substrate drives the LED to emit NIR photons, which can be detected by a low-cost CCD. As a proof of concept, we have demonstrated X-ray detection and presented preliminary imaging results, providing another example of the applicability of the PD-LED design for optical frequency conversion. This down-conversion method of imaging eliminates the need for connecting readout circuits, therefore lowering the production cost and simplifying the manufacturing process. This PD-LED architecture leverages mature materials and fabrication processes and offers an alternative approach to X-ray detection and imaging. It has the potential to achieve devices with higher absorption, improved image resolution, and enhanced material stability.

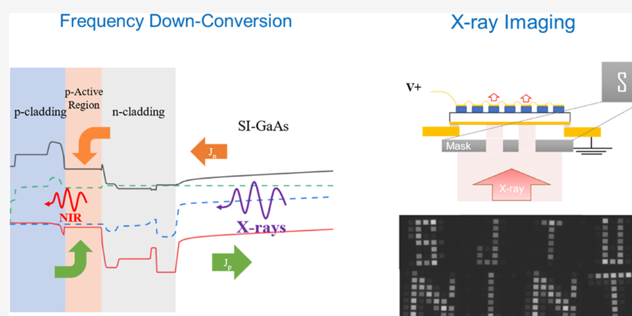

KEYWORDS: *frequency down-conversion, X-ray detection, X-ray imaging, light-emitting diodes, semi-insulating GaAs*

■ INTRODUCTION

As one of the most important light-emitting devices, light-emitting diodes (LEDs) are widely used in medical imaging,[1] biosensing,[2] optical communications,[3,4] and night vision.[5] In the near-infrared (NIR) band, GaAs-based LEDs are of significant importance, attributed to their well-established material and processing technologies, simple structure, and low price. GaAs-based LEDs can be grown on GaAs substrates of different doping types, including n-type and p-type,[6] as well as semi-insulating GaAs (SI-GaAs) substrates. It is noted that SI-GaAs is an excellent material for X-ray detection[7] because of high absorption.[8,9]

Since GaAs-based infrared LEDs can be epitaxially grown on SI-GaAs substrates and the light emitted by the LEDs can be detected by a low-cost CCD directly, it naturally leads us to consider whether LEDs with SI-GaAs substrates can be directly used for X-ray detection and imaging. X-rays ionize and produce photogenerated charge carriers in the SI-GaAs. Under the influence of the electric field, these carriers move directionally to form a photocurrent, which drives the LED to emit NIR photons. The emission can be directly observed using an infrared camera, thus achieving X-ray detection/imaging. This actually utilizes a frequency conversion detection and imaging mechanism, which has been successfully applied in the infrared band with several examples.[10−16] By integrating different types of photodetectors (PDs) with an LED, infrared as well as terahertz imaging[17] were realized. Considering the possibility of using an SI-GaAs substrate as the PD for X-ray detection, a frequency down-conversion process can be realized by converting X-rays to NIR photons. It is not difficult to find that such a kind of imaging scheme shows an obvious advantage since it does not need to connect readout circuits and has the potential to achieve pixel-less imaging using a large single imaging unit, therefore simplifying the manufacturing complexity. In contrast, the traditional GaAs X-ray direct imaging detectors needed to be integrated with readout circuits[18,19] to achieve efficient and high-resolution X-ray imaging. The proposed scheme is similar to conventional scintillation detectors[20,21] in that it belongs to the category of indirect imaging schemes. However, it differs significantly from scintillators in that it does not exhibit an afterglow effect.

Received: June 23, 2025
Revised: October 10, 2025
Accepted: October 13, 2025
Published: October 20, 2025

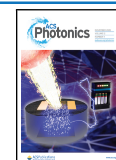

 © 2025 American Chemical Society

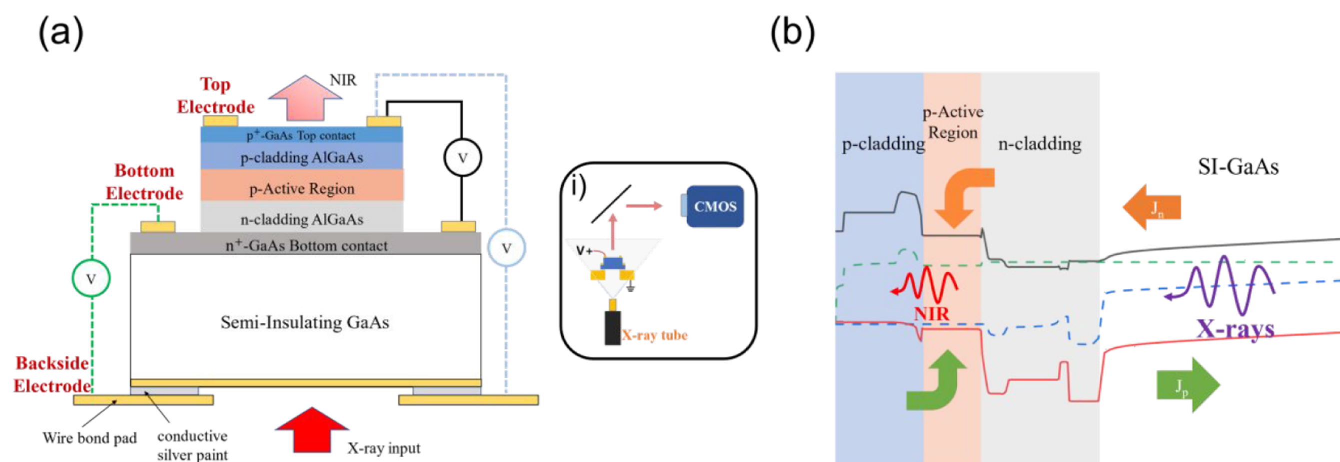

Figure 1. Device structure and operating mechanism. (a) Schematic of the device structure; (i) inset is experimental setup for X-ray detection/imaging. (b) Band diagram and mechanism of the frequency down-conversion process.

In this article, we introduce an alternative detection/imaging method that differs completely from traditional X-ray detection/imaging schemes. Utilizing the mechanism of frequency down-conversion, a simple infrared LED with an SI-GaAs substrate is employed as an X-ray detection/imaging device. Preliminary imaging results are obtained by etching through the heavily doped bottom contact layer. This proposed X-ray detection configuration not only is simple but also capitalizes on the properties of SI-GaAs, a commercially accessible X-ray detection material known for its high absorption and spatial resolution capabilities. Our result demonstrates the wide applicability of the PD-LED design for optical frequency conversion, and we hope it will provide alternative options for future applications.

RESULTS

Device Structure and Operation Mechanism. The schematic structure of the device is shown in Figure 1a. This LED material is epitaxially grown on a 625 μm SI-GaAs substrate in sequence: the highly doped n^+-GaAs bottom contact layer, the n-AlGaAs cladding layer, the p-active region, the p-AlGaAs cladding layer, and the highly doped p^+-GaAs top contact layer. By the standard photolithography and wet etching processes, square mesas with sizes of 1 mm × 1 mm and 3 mm × 3 mm were fabricated. The mesa is etched into the bottom contact layer. We deposited Ti/Pt/Au on the p-type-doped top contact layer and AuGe/Ti/Pt/Au on the n-type-doped bottom contact layer to ensure ohmic contact. Ti/Pt/Au was deposited on the backside of the SI-GaAs substrate to form a Schottky backside electrode. The backside of the device was glued onto a PCB holder with conductive silver paint, which has a window to allow for X-rays to be incident on the device from the backside. Detailed parameters of the LED are shown in Figure S1. This epitaxial structure refers to the GaAs/AlGaAs LED described by D. Ban et al.[22] The active region is composed of 400 nm Be-doped GaAs with a doping concentration of 1.0×10^{18} cm^{-3}, which is sandwiched between n-type and p-type cladding layers.

Considering the presence of three electrodes—namely, the top, bottom, and backside electrodes—there are three distinct testing modes designed to measure the characteristics of the SI-GaAs photodetector, the LED, and the X-ray down-conversion process, respectively, as depicted in Figure 1a. To solely measure the response of the SI-GaAs to X-rays, a bias was applied between the bottom and backside electrodes, with the bottom electrode being positive. When evaluating the LED's performance, a bias was applied across the top and bottom electrodes, with the top electrode being positive. This setup ensures that the LED is under forward bias, allowing us to examine its electroluminescent properties. For the X-ray down-conversion measurement, we applied a bias between the top electrode and the backside electrode, with the top electrode being positive to forward-bias the LED.

The schematic experimental setup is shown in the inset of Figure 1a. The entire setup is placed in a darkroom made from lead-lined panels. X-ray is generated by an X-ray tube (MOXTEK ULTRA-LITE MAGNUM) 1.5 cm away from the sample. The intensity of the X-ray is controlled by the tube voltage U_{tube} and tube current I_{tube}, which is proportional to I_{tube}, approximately quadratically related to U_{tube}, and inversely proportional to the square of the distance. With a tube voltage of 30 kV and a tube current of 100 μA, the calibrated radiation dose rate at a distance of 2 cm from the head of the X-ray tube is 0.383 Gy·s^{-1}. Through the back window of the PCB holder, the X-rays are irradiated on the SI-GaAs substrate. The emitting light from the LED is reflected by a 45° mirror and observed on the other side with the IR camera (Photonic Science cooled sCMOS).

The operation mechanism of the device can be understood in terms of the energy band diagram shown in Figure 1b. When the device operates in the X-ray down-conversion mode, the voltage mainly drops across the SI-GaAs region since the LED is forward-biased. Upon X-ray irradiation, a large number of electron−hole pairs are generated in the SI-GaAs substrate. Under the electric field formed by the bias voltage, these carriers move directionally, i.e., electrons move toward the LED region and holes move in the opposite direction, forming both electron and hole currents. Electrons injected into the active region of the LED recombine radiatively with holes injected from the other side, thus emitting NIR photons. The transformation of X-ray photons to NIR photons within the device is a frequency down-conversion process.

X-ray Detection. To investigate the performance of the down-conversion X-ray detector, understanding the characteristics of the SI-GaAs substrate as a PD and the LED is necessary. In the following, we first measure the performance of the SI-GaAs substrate and the LED. The size of the tested device is 1 mm × 1 mm.

https://doi.org/10.1021/acsphotonics.5c01458
ACS Photonics 2025, 12, 6028−6036

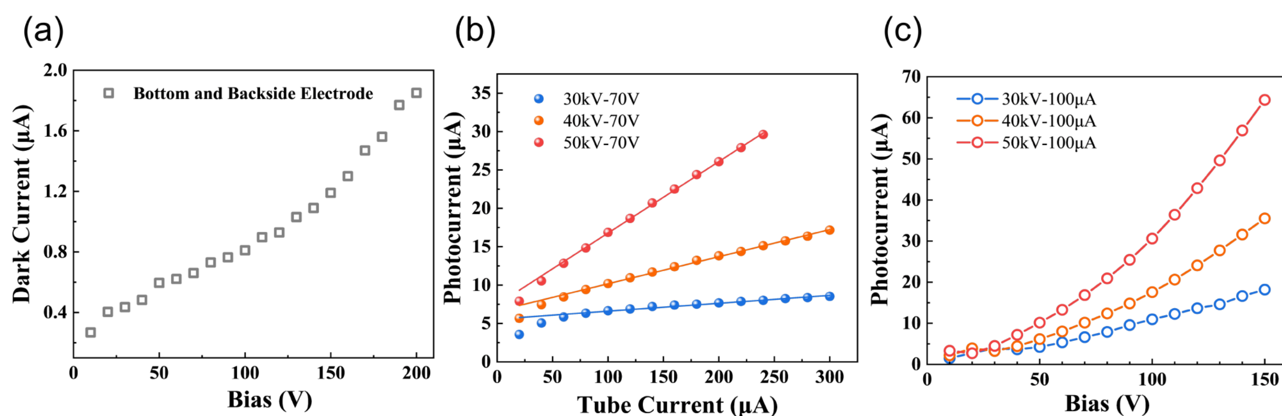

Figure 2. Dark current and photocurrent response of the SI-GaAs. (a) Dark current characteristics of the SI-GaAs substrate as a PD. (b) The dependence of photocurrent of the SI-GaAs substrate on the X-ray tube current, when U_{bias} = 70 V, and U_{tube} = 30 kV, 40 kV, 50 kV. (c) The dependence of photocurrent of the SI-GaAs substrate on the bias under three different X-ray intensities: (U_{tube} = 30 kV, I_{tube} = 100 μA), (U_{tube} = 40 kV, I_{tube} = 100 μA), (U_{tube} = 50 kV, I_{tube} = 100 μA).

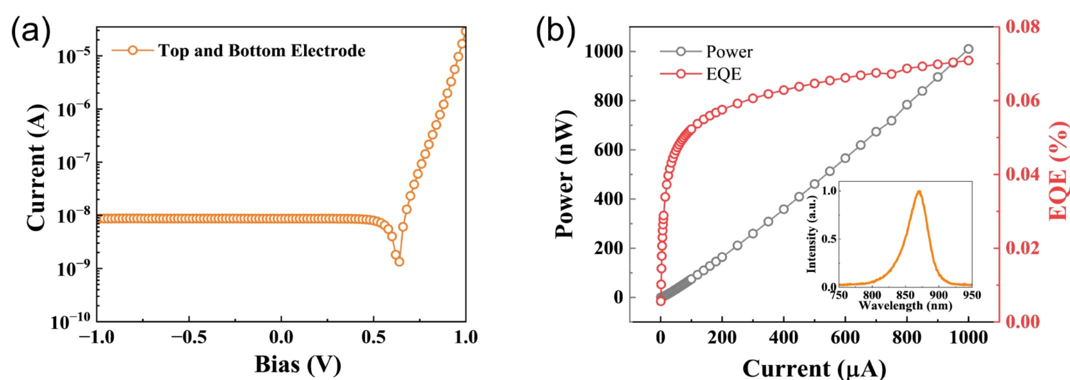

Figure 3. Performance of the GaAs/AlGaAs LED. (a) $I-V$ characteristics of the LED, biasing the top and bottom electrodes. (b) External quantum efficiency (EQE) and optical power versus current of the LED. The inset is the emission spectrum of the LED.

Figure 2a presents the dark current characteristics of the SI-GaAs substrate as a PD, where the bottom electrode and the backside electrode are biased. The SI-GaAs substrate exhibited high resistance without X-ray irradiation. The dark current is below 2 μA, even when the applied voltage is up to 200 V. Under X-ray irradiation, photocurrent is generated, which could be influenced by the tube current I_{tube} and tube voltage U_{tube} as well as the bias. Figure 2b shows the linear dependence of the photocurrent on the tube current under different tube voltages when the bias of the device is 70 V. The slight deviation from linearity at tube currents less than 50 μA may be attributed to the X-ray tube's tungsten filament not reaching a high enough temperature when operating at low current. Because the intensity of X-rays is proportional to the tube current and the generated photocurrent is also proportional to the X-ray intensity, the linearity observed in the graph is reasonable. It is noted that the higher the tube voltage, the stronger the generated photocurrent. Additionally, the photocurrent varies with the bias voltage of the device. As shown in Figure 2c, three different X-ray intensities were used: (U_{tube} = 30 kV, I_{tube} = 100 μA), (U_{tube} = 40 kV, I_{tube} = 100 μA), and (U_{tube} = 50 kV, I_{tube} = 100 μA). With increasing bias, the electric field across the SI-GaAs becomes stronger, leading to higher collection efficiency of the carriers generated by the X-rays and consequently a larger photocurrent. It should be noted that due to the very high resistance of the SI-GaAs substrate, the dark current of the SI-GaAs substrate PD is almost negligible compared to the photocurrent, which indicates that light emission of the LED is mainly driven by the photocurrent. The SI-GaAs substrate in use has a thickness of ~600 μm and a resistivity of 1×10^{18} Ω·cm. Employing SI-GaAs with higher resistivity could further reduce the dark current. Besides, reducing the substrate thickness (while ensuring it is no less than the X-ray absorption length) would increase the photocurrent under the same bias voltage, as the electric field within the SI-GaAs region will be increased.

To study the properties of the LED, we apply a bias between the top and bottom electrodes. Figure 3a shows the $I-V$ curve of the LED alone. It clearly exhibits rectification characteristics, indicating that the LED structure can be simply seen as a p−n junction diode. Figure 3b demonstrates the dependence of the optical power as well as the external quantum efficiency (EQE) on the driving current. It can be seen that the light emission power is directly proportional to the driving current, with the emission peak at around 870 nm. The external quantum efficiency is a key parameter to characterize the performance of an LED, which is defined as the ratio of the number of outgoing photons to that of the electrons injected into the LED. The rapid increase in EQE between 0 and 100 μA is mainly attributed to the substantial increase in radiative efficiency under low current injection. In this regime, the radiative recombination rate increases faster than the SRH (Shockley-Read-Hall) recombination rate, leading to a significant increase in radiative efficiency. Considering the

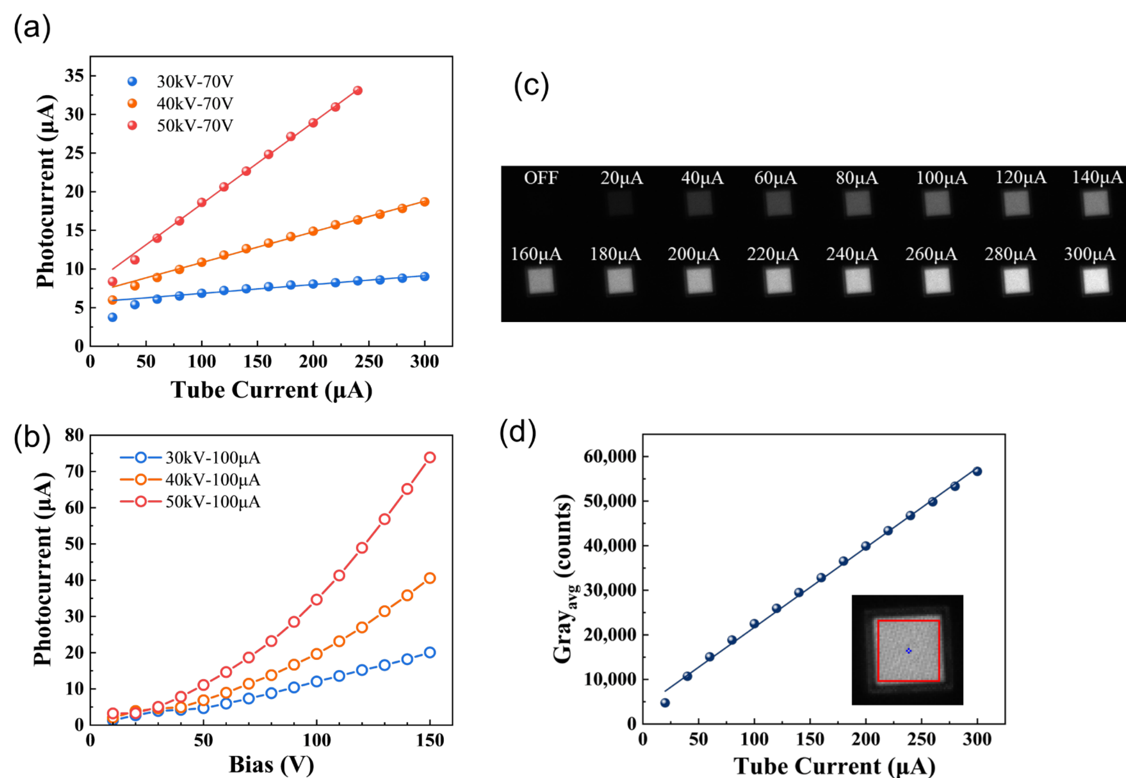

Figure 4. Photocurrent response and down-converted luminance of the device. (a) Photocurrent response to X-ray tube current at U_{bias} = 70 V, when U_{tube} is 30 kV, 40 kV, 50 kV, respectively. (b) The dependence of photocurrent on the bias, when I_{tube} is 100 μA and U_{tube} is 30 kV, 40 kV, 50 kV, respectively. (c) Infrared photographs of the luminescence produced by a 1 mm device under X-ray irradiation with different I_{tube}, when U_{bias} = 150 V and U_{tube} = 40 kV. (d) The average grayscale values of the above infrared photographs under different I_{tube}.

bias, the tube voltage, and the tube current for device operation, the photocurrent generated by SI-GaAs is about tens of μA, leading to the light output power of about 10−70 nW, and the EQE is about 0.05%. The low EQE is due to the device operating at a low driving current, where the internal quantum efficiency of the LED is not high and is dominated by SRH recombination processes.[22,23] The EQE can be significantly increased through improvements in material quality and the implementation of surface microstructures on the LED. Though the EQE is not high, it is sufficient to observe the frequency down-conversion process.

Based on the investigation of the SI-GaAs substrate (as a PD) and of the LED, we further studied the characteristics of the device as a frequency down-conversion X-ray detector by applying the bias between the top and backside electrodes. The dark current is below 2 μA under 200 V, similar to the result of SI-GaAs (Figure 2a), and the photocurrent response to X-rays shown in Figure 4a,b is also highly similar to that of SI-GaAs (Figure 2b,c). This indicates that the SI-GaAs substrate is the main region where photocurrent is generated and the voltage drops. The SI-GaAs substrate of the LED can indeed function as a PD, which generates photocurrent and drives the LED.

Through the frequency down-conversion process, the X-ray detection was realized by capturing the luminescence of the LED using an infrared camera, as shown in Figure 4c. This figure displays a set of images of a 1 mm-sized mesa under X-ray irradiation of different tube currents (20 μA to 300 μA) when the bias voltage is 150 V and U_{tube} is 40 kV. The image of the device without X-ray irradiation is also presented, and no LED emission can be observed through the camera because of the low dark current (<2 μA). The integration time of the camera is 30 ms. It can be observed that the infrared luminescence of the down-conversion device becomes stronger as the X-ray intensity increases. The minimum emitted optical power of the LED that can be observed by the infrared camera is about 0.6 nW, which requires the driving current to be at least 3 μA. It indicates that without X-ray irradiation, no LED emission can be observed through the camera because of the low dark current (<2 μA). During the experiment, we did not observe any significant degradation of the device performance from X-ray irradiation. Based on the relevant results,[24−26] we believe that the device should be radiation-hard to X-ray irradiation. Nevertheless, comprehensive investigations on the material and device stability should be carried out in future work. The average grayscale value ($Gray_{avg}$) of the above infrared photos is also examined, as shown in Figure 4d. The value is calculated by averaging the grayscale value in the 1 mm area (indicated in red) of the infrared photo. It can be seen that $Gray_{avg}$ varies linearly with tube current, as the photocurrent does. During the frequency down-conversion experiment, we also monitored the voltage drop across the LED (U_{LED}). Under a 70 V bias condition, the device exhibited a dark current of 0.584 μA and a U_{LED} of 0.826 V. When subjected to X-ray irradiation with varying intensities, the generated photocurrent ranged from 4 to 17 μA, and the U_{LED} varied from 0.92 to 0.97 V. The result confirms the series configuration of the LED and the SI-GaAs substrate, demonstrating that the magnitude of the photocurrent generated in the SI-GaAs directly determines the voltage drop across the LED.

So far, we have demonstrated that X-ray detection could indeed be realized with a simple LED by a frequency down-

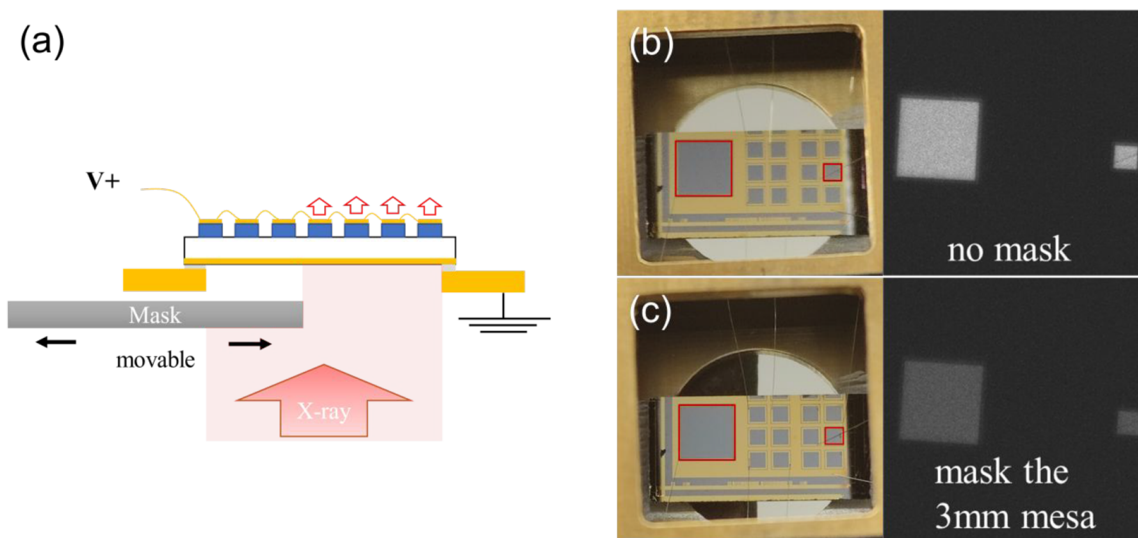

Figure 5. Experimental setup and lateral current conduction of the device retaining the bottom contact layer. (a) Schematic experimental setup for spatial resolution testing. All the mesas share the same bottom contact layer. (b) The actual image (left) and corresponding IR image (right) of the device with no mask. The two parallel-connected mesas (one 3 mm mesa and one 1 mm mesa) are marked in red. (c) The actual image (left) and IR image (right) after masking the 3 mm mesa.

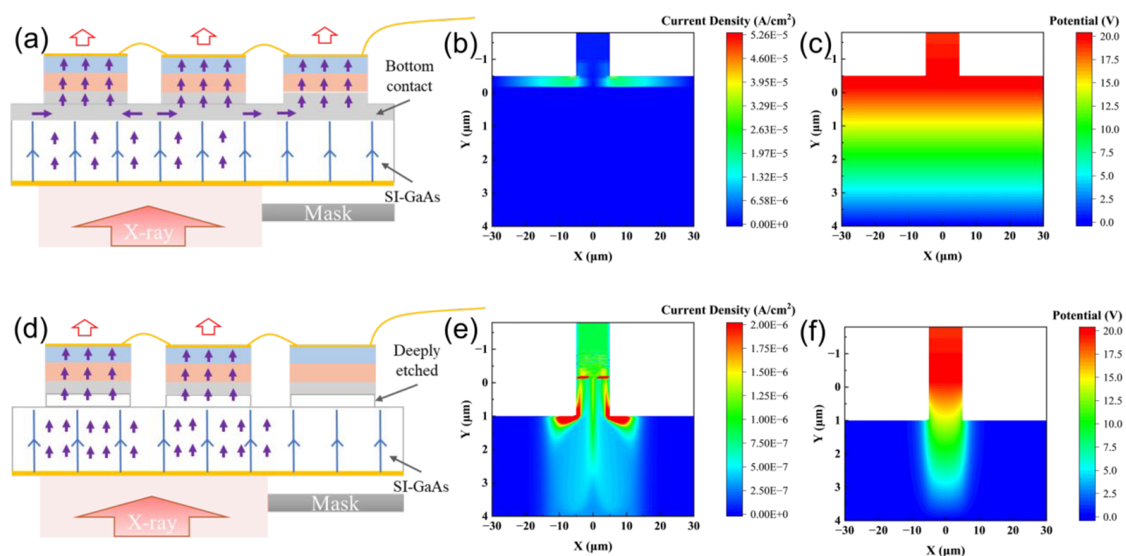

Figure 6. Simulation of the effect of the bottom contact layer on lateral current conduction. (a) Schematic diagram of the photocurrent distribution in the device retaining the bottom contact layer. (b) Current density in the device retaining the bottom contact layer. (c) Electric potential in the device retaining the bottom contact layer. (d) Schematic diagram of the photocurrent distribution in the device with the bottom contact layer etched away. (e) Current density in the device with the bottom contact layer etched away. (f) Electric potential in the device with the bottom contact layer etched away.

conversion mechanism. Whether this device can be used for imaging is still an open question. In the following, the capability of X-ray spatial resolution was studied.

X-ray Imaging. To verify if such a down-conversion X-ray detector can be used for imaging, the capability for X-ray spatial resolution is investigated. The schematic diagram of the experiment setup is shown in Figure 5a. The mesas are connected in parallel using gold wires. A movable mask is utilized to block the X-rays incident on the sample, resulting in some mesas not being irradiated by X-rays, while others are. We expect that only the irradiated mesas would emit light if they have spatial resolution. Based on such consideration, we fabricated multiple mesas on the same epitaxial wafer. We connected two mesas with sizes of 3 mm and 1 mm in parallel, as indicated in red in Figure 5b,c. The down-conversion X-ray-to-infrared luminescence without a mask is shown in Figure 5b, where both mesas glow simultaneously. In contrast, the down-conversion infrared photograph of the 3 mm mesa blocked from X-rays is presented in Figure 5c. Contrary to our expectation, even though the 3 mm mesa was masked, both the 3 and 1 mm mesas glowed simultaneously regardless of whether they were blocked or not. This indicates that such a structure lost the spatial resolution of imaging. The current driving the 3 mm mesa was laterally conducted from the unmasked portion. Due to the masking, the total photocurrent generated was smaller; hence, the infrared luminous intensity was also weaker compared to the no-mask scenario.

https://doi.org/10.1021/acsphotonics.5c01458
ACS Photonics 2025, 12, 6028−6036

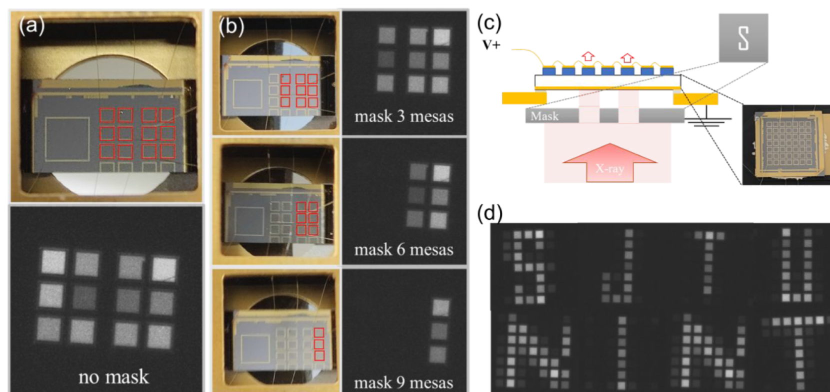

Figure 7. Spatial resolution results for the structure with the bottom contact layer etched away, showing the actual devices and corresponding down-conversion infrared photographs. (a) The actual device image and IR photograph, with 12 parallel-connected 1 mm mesas. (b) Different numbers of masked mesas are shown, masking 3, 6, and 9 mesas from top to bottom, respectively. (c) A 7 × 7 array device for down-converted imaging, with each mesa size of 1 mm^2, using a letter-shaped mask to block the incident X-rays. (d) Infrared photographs of down-converted imaging after blocking X-rays with different letter-shaped masks.

To understand why the device lost the capability of spatial resolution, we inspect the epitaxial structure and the fabrication process. It is noted that all of the mesas share the common bottom contact layer. Due to the high doping and low resistance of this layer, the photocurrent will be easily conducted laterally in the bottom contact layer. Figure 6a shows the schematic photocurrent distribution in the device when multiple mesas are connected in parallel and the device is partially masked from X-rays. Due to the high conductivity of the bottom contact layer, the electric field across the SI-GaAs region is uniform when biased. Upon irradiation with X-rays, a large number of photogenerated carriers are produced in the unmasked area of the SI-GaAs. These carriers drift under the uniform electric field and reach the bottom contact layer. So far, the spatial information has not yet been lost. Once the carriers reach the bottom contact layer, due to the high conductivity of the p-doped contact layer, the photocurrent will conduct laterally, leading to a redistribution of the current, with the final effect of making all the parallel-connected mesas glow simultaneously. To verify this assumption, we simulate the current distribution of a single mesa, and there is obvious lateral spreading of the current in the bottom contact layer, as shown in Figure 6b. The potential distribution is shown in Figure 6c, which is laterally uniform in this geometry. It indicates that a uniform electric field is distributed in the SI-GaAs. This structure is analogous to a planar capacitor, with the highly doped layer and the backside metal serving as the two metal plates and the SI-GaAs in between acting as the dielectric layer.

The lateral conduction effect of the bottom contact layer can also be inferred from the magnitude of the photocurrent. We measure the photocurrent of 1 and 3 mm mesas using the X-ray with the same intensity, respectively. The photocurrent is almost equal in magnitude. The results are shown in Figure S2. The resulting photocurrent is even the same as that measured by the SI-GaAs substrate (biasing the bottom electrode and backside electrode). If the device had spatial resolution, the photocurrent collected by the 3 mm mesa would be larger than that of the 1 mm mesa, but this is not the case. This is actually due to the fact that the presence of the bottom contact layer collects the photocurrent generated by the entire SI-GaAs substrate and injects it into a single mesa; therefore, the magnitude of the current is independent of the size of that mesa.

In order to eliminate the impact of the bottom contact layer on the current conduction, we increased the etch depth of the mesas, etching through the highly conductive common bottom contact layer and revealing highly resistive SI-GaAs. The modified structure is shown in Figure 6d. The etching depth of all the mesas exceeds the thickness of the epitaxial layer and reaches the SI-GaAs region. The mesas are now electrically isolated from each other, as they are separated by high-resistivity SI-GaAs and no longer connected by a highly conductive bottom contact layer. In this deeply etched structure, the mesas are able to collect the photocurrent at the corresponding position without significant current spreading. Figure 6e shows the corresponding simulation results. It can be seen that the current distribution is more concentrated under the mesas, and the lateral current spreading is significantly suppressed due to the existence of an electrical isolation region. In Figure 6f, the simulated potential drops mainly in the region below the mesa, which indicates that the electric field in this region is more concentrated, and this localization enables the mesa to collect the photocurrent at the corresponding position.

In contrast, the collected photocurrent in the deeply etched structure is measured. Figure S3 gives the magnitudes of the collected photocurrent of one 3 mm mesa and one 1 mm mesa. It is seen that the magnitude of the photocurrent is now correlated to the area of the mesa. Additionally, the photocurrent is lower than that of the structure with the common bottom contact layer. These results indicate that the deeply etched structure no longer collects photocurrent generated at other positions, and current spreading is effectively suppressed.

We performed X-ray spatial resolution tests on a deeply etched device. Twelve mesas of 1 mm size in parallel with gold wires are connected, as marked in red in Figure 7a. The down-converted luminescence of these 12 mesas irradiated by X-ray without a mask is shown in the infrared photo below. Using a mask to cover different portions of the device, we obtained infrared photographs with different numbers of luminous mesas; see Figure 7b. From top to bottom, 3, 6, and 9 mesas were masked, and the IR photos show the corresponding luminance. This shows that etching through the common

https://doi.org/10.1021/acsphotonics.5c01458
ACS Photonics 2025, 12, 6028−6036

bottom contact layer can greatly suppress the lateral current conduction and restore the spatial resolution capability of X-rays. It should be noted that the total thickness of the device is ~600 μm. Compared with the case of the QWIP-LED[12,13] with the thickness of ~10 μm, the thickness of our down-conversion X-ray detector is much thicker. It indicates that the spatial information on the light field could be retained well at this thickness as long as the resistance is high enough, proving the ubiquity of the frequency conversion imaging scheme.

To further investigate the imaging ability of the device, we fabricated an array-like device with more mesas, each of which is 1 mm in size, forming a 7 × 7 array, and the top electrodes of each mesa were connected in parallel via gold wires, enabling all mesas to be biased simultaneously. The actual shape of the device is shown in the inset of Figure 7c. A mask with an alphabetic shape is placed at the back of the device to block the X-ray. The down-converted luminescence of the device also shows the shape of the corresponding letter, as seen in Figure 7d. Here, we used down-converted imaging photos of different alphabetic characters to compose this figure.

In Figure 7d, we can observe a distinct luminescence from the mesa irradiated by an X-ray. However, it is also noted that there are some lightly glowing mesas at the edges of the letters, indicating that there is still some electric crosstalk. When collecting the photocurrent, some current flows into the mesa not irradiated by X-rays, resulting in a weak glowing. Although we have removed the bottom contact layer, which is the main conduction layer, the semi-insulating substrate can still laterally conduct the current to some extent, as shown in Figure 6e where the current collecting area is larger than the mesa. This diffusion effect may be suppressed by using an SI-GaAs substrate with a higher resistivity and thinner thickness or by decreasing the operating temperature of the device. Additionally, the device has some malfunctional mesas that will not glow at all, and the brightness between the mesas is not uniform. This may be related to defects, crystal growth quality, and sophistication of the manufacturing process. These challenges are also encountered in up-conversion pixel-less imaging devices. Fabricating such devices need large areas of material without severe defects. However, in the case of such an array imaging, the defects only render individual mesas inoperable while the rest can still operate normally, but in infrared up-conversion pixel-less imaging, there is only one large imaging unit; severe defects would cause the entire device to fail. Therefore, this array-like pixelated PD-LED configuration is more tolerant to defects. Furthermore, the current mesa area demonstrated is 1 mm^2. If we increase the number of pixels and make them denser, then a higher imaging resolution could be realized.

As originally conceived, such frequency conversion devices can be used for pixel-less imaging similar to the up-conversion results of QWIP-LED.[12,13] So, we performed detailed tests on a 3 mm mesa of a deeply etched structure (see Figure S4). Unfortunately, we failed to achieve pixel-less imaging. Within the large-sized mesa, the luminance was uniform, and the spatial information was lost. The highly doped layer in the mesa again acted as a current spreading layer. Another possible reason why we failed to achieve pixel-less imaging is that our device operates at room temperature and carriers have a large diffusion coefficient, whereas QWIP-LEDs operate at liquid nitrogen temperature. By cooling down the device, we may restore the spatial information inside the mesa and achieve pixel-less imaging. Alternatively, the common region of the LED and SI-GaAs could be improved, for instance, by fabricating an i-n-i common region.[14,27] By reduction of the doping concentration of the bottom contact layer to suppress the lateral current conduction, it may also be possible to achieve pixel-less imaging.

DISCUSSION

As one of the most important light-emitting devices in the near-infrared band, GaAs-based LED shows high performance, well-established manufacturing processes, and reduced production costs. In this paper, we have demonstrated an alternative application of a simple GaAs-based LED with an SI-GaAs substrate for X-ray detection and imaging. The underlying mechanism involves semiconductor frequency down-conversion, where the SI-GaAs substrate serves as a detector. When exposed to X-rays, the SI-GaAs substrate generates photocurrent that drives the LED to emit NIR photons, which are subsequently detected using an infrared camera. This approach offers several advantages, including the elimination of the need for a readout circuit, thereby simplifying manufacturing complexity. The device exhibits a linear response to X-rays and operates efficiently at room temperature.

Furthermore, we explored the role of the heavily doped bottom contact layer of the LED in current conduction. By increasing the etching depth, we have significantly reduced its impact on imaging, achieving preliminary X-ray imaging results. This work provides another example of the applicability of the PD-LED design for optical frequency conversion. To improve the imaging performance, we suggest fabricating devices with higher pixel densities using current array fabrication technologies. Utilizing higher-resistivity SI-GaAs substrates can simultaneously improve spatial resolution in high-pixel-density arrays while suppressing dark current. Further architectural optimizations—such as implementing a passivation layer to reduce the sidewall leakage current—can also enhance device performance. Additionally, incorporating microstructures on the surface could increase the light extraction efficiency. These combined measures are expected to significantly enhance the sensitivity and overall signal-to-noise ratio. Alternatively, to fabricate a large-area pixel-less imaging detector, the connection region between the LED and the SI-GaAs should be specially designed. For instance, an intrinsic-n-intrinsic (i-n-i) common region would be feasible. Reducing the doping concentration and the thickness of the highly doped bottom contact layer could suppress lateral current conduction, potentially enabling pixel-less imaging.

Although this paper presents only preliminary imaging results, the advantages of such a down-conversion X-ray detector in imaging are noteworthy. First, the down-conversion method eliminates the need for connecting readout circuits, and the image can be captured by an infrared CCD. The flip-chip bonding process to align indium bumps to readout circuits could be avoided, and it would greatly lower the production cost and simplify the manufacturing processes. Second, it is based on the mature III−V material and fabrication processing. As a commercial X-ray detection material, the SI-GaAs material itself offers high absorption and spatial resolution capabilities. Compared with traditional scintillators, such as CsI(Tl),[28] NaI(Tl),[29] $Bi_4Ge_3O_{12}$ (BGO),[30] and (Lu,Y)SiO_5,[31] SI-GaAs not only exhibits excellent stability and optoelectrical properties but also is nontoxic and environmentally friendly. More importantly, it

https://doi.org/10.1021/acsphotonics.5c01458
ACS Photonics 2025, 12, 6028−6036

may not suffer from the afterglow effect. Third, the frequency down-conversion concept of the PD-LED design used in this work can be flexibly extended to other material systems. For example, it can be used to achieve down-conversion from X-rays to visible light using inorganic semiconductors like GaN[32,33] or by integrating OLEDs with SI-GaAs to create hybrid X-ray-to-visible-light down-conversion devices. Thereby, the image can be detected by the naked eye or CCDs. Leveraging the low lateral diffusion characteristics of carriers in organic materials[34] and the advantages of solution-based[35,36] fabrication, it will be easier to produce large-area, pixel-less imaging devices. We believe that, based on the PD-LED architecture, it is possible to fabricate X-ray imaging devices with higher absorption, improved image resolution, and enhanced material stability.

■ ASSOCIATED CONTENT

Supporting Information

The Supporting Information is available free of charge at https://pubs.acs.org/doi/10.1021/acsphotonics.5c01458.

> Detailed parameters of epitaxial LED (Figure S1); comparison of photocurrent collection capability (Figures S2 and S3); spatial resolution results for a 3 mm mesa device (Figure S4) (PDF)

■ AUTHOR INFORMATION

Corresponding Authors

Wenzhong Shen − *Key Laboratory of Artificial Structures and Quantum Control, School of Physics and Astronomy, Shanghai Jiao Tong University, Shanghai 200240, China;* orcid.org/0000-0003-4527-9183; Email: wzshen@sjtu.edu.cn

Liang Chen − *Radiation Detection Research Center, Northwest Institute of Nuclear Technology, Xi'an 710024, People's Republic of China;* orcid.org/0009-0007-8108-3598; Email: Chenl_nint@163.com

Yueheng Zhang − *Key Laboratory of Artificial Structures and Quantum Control, School of Physics and Astronomy, Shanghai Jiao Tong University, Shanghai 200240, China;* orcid.org/0000-0002-1702-5680; Email: yuehzhang@sjtu.edu.cn

Authors

Quan Yu − *Key Laboratory of Artificial Structures and Quantum Control, School of Physics and Astronomy, Shanghai Jiao Tong University, Shanghai 200240, China*

Fangbao Wang − *Radiation Detection Research Center, Northwest Institute of Nuclear Technology, Xi'an 710024, People's Republic of China*

Xin Yuan − *Key Laboratory of Artificial Structures and Quantum Control, School of Physics and Astronomy, Shanghai Jiao Tong University, Shanghai 200240, China*

Ying Liu − *Key Laboratory of Artificial Structures and Quantum Control, School of Physics and Astronomy, Shanghai Jiao Tong University, Shanghai 200240, China*

Lianghua Gan − *Key Laboratory of Infrared Imaging Materials and Detectors, Shanghai Institute of Technical Physics, Chinese Academy of Sciences, Shanghai 200083, China*

Gangyi Xu − *Key Laboratory of Infrared Imaging Materials and Detectors, Shanghai Institute of Technical Physics, Chinese Academy of Sciences, Shanghai 200083, China; Hangzhou Institute for Advanced Study, University of Chinese Academy of Sciences, Hangzhou 310024, China;* orcid.org/0000-0002-9004-030X

Complete contact information is available at: https://pubs.acs.org/10.1021/acsphotonics.5c01458

Author Contributions

L.C. and Y.Z. conceived the idea. Q.Y. performed the numerical simulations, fabricated the device, and carried out the experiment. F.W. established the experimental setup and helped with the measurements. X.Y., Y.L., L.G., and G.X. helped with device fabrication. Q.Y., Y.Z., and L.C. discussed the results and wrote the manuscript. L.C., Y.Z., W.S., and G.X. reviewed the manuscript. All authors have given approval to the final version of the manuscript.

Funding

This work was supported by the National Natural Science Foundation of China (12274285, 12305205, 62204198, 12393833, 62435020, 62235010) and the Shanghai New Energy Technology Research and Development Project, China (24DZ3000900).

Notes

The article was previously submitted to a preprint server.[37]
The authors declare no competing financial interest.

■ REFERENCES

(1) Medintz, I. L.; Uyeda, H. T.; Goldman, E. R.; Mattoussi, H. Quantum Dot Bioconjugates for Imaging, Labelling and Sensing. *Nat. Mater.* **2005**, *4* (6), 435−446.

(2) Lee, H.; Lee, W.; Lee, H.; Kim, S.; Alban, M. V.; Song, J.; Kim, T.; Lee, S.; Yoo, S. Organic−Inorganic Hybrid Approach to Pulse Oximetry Sensors with Reliability and Low Power Consumption. *ACS Photonics* **2021**, *8* (12), 3564−3572.

(3) He, F.; Song, E.; Zhang, C.; Chang, H.; Dong, G.; Xia, Z.; Wang, W.; Zhang, Q. Cr^{3+} ↔Fe^{3+} Energy Transfer Offset Enabling Anti-Thermal Quenching Near-Infrared Emission for Coded Wireless-Communication Applications. *Laser Photonics Rev.* **2024**, *18* (3), 2300668.

(4) Minotto, A.; Haigh, P. A.; Łukasiewicz, Ł. G.; Lunedei, E.; Gryko, D. T.; Darwazeh, I.; Cacialli, F. Visible Light Communication with Efficient Far-Red/near-Infrared Polymer Light-Emitting Diodes. *Light: Sci. Appl.* **2020**, *9* (1), 70.

(5) Wang, Z.; Wei, Y.; Ren, Z.; Wang, W.; Tu, D.; Li, G. Simultaneous Luminescence Color Tuning and Spectral Broadening of Cr3+ Near-Infrared Emission for Night Vision Application. *ACS Appl. Opt. Mater.* **2023**, *1* (6), 1088−1096.

(6) Liu, L.; Edgar, J. H. Substrates for Gallium Nitride Epitaxy. *Mater. Sci. Eng., R* **2002**, *37* (3), 61−127.

(7) McGregor, D. S.; Hermon, H. Room-Temperature Compound Semiconductor Radiation Detectors. *Nucl. Instrum. Methods Phys. Res., Sect. A* **1997**, *395* (1), 101−124.

(8) Fiederle, M.; Procz, S.; Hamann, E.; Fauler, A.; Fröjdh, C. Overview of GaAs Und CdTe Pixel Detectors Using Medipix Electronics. *Cryst. Res. Technol.* **2020**, *55* (9), 2000021.

(9) Procz, S.; Roque, G.; Avila, C.; Racedo, J.; Rueda, R.; Santos, I.; Fiederle, M. Investigation of CdTe, GaAs, Se and Si as Sensor Materials for Mammography. *IEEE Trans. Med. Imaging* **2020**, *39* (12), 3766−3778.

(10) Liu, H. C.; Allard, L. B.; Buchanan, M.; Wasilewski, Z. R. Pixelless Infrared Imaging Device. *Electron. Lett.* **1997**, *33* (5), 379−380.

(11) Allard, L. B.; Liu, H. C.; Buchanan, M.; Wasilewski, Z. R. Pixelless Infrared Imaging Utilizing a P-Type Quantum Well Infrared Photodetector Integrated with a Light Emitting Diode. *Appl. Phys. Lett.* **1997**, *70* (21), 2784−2786.

(12) Dupont, E.; Byloos, M.; Gao, M.; Buchanan, M.; Song, C.-Y.; Wasilewski, Z. R.; Liu, H. C. Pixelless Thermal Imaging with Integrated Quantum-Well Infrared Photodetector and Light-Emitting Diode. *IEEE Photonics Technol. Lett.* **2002**, *14* (2), 182−184.
(13) Dupont, E.; Byloos, M.; Oogarah, T.; Buchanan, M.; Liu, H. C. Optimization of Quantum-Well Infrared Detectors Integrated with Light-Emitting Diodes. *Infrared Phys. Technol.* **2005**, *47* (1−2), 132−143.
(14) Luo, H.; Ban, D.; Liu, H. C.; Poole, P. J.; Buchanan, M. Pixelless Imaging Device Using Optical Up-Converter. *IEEE Electron Device Lett.* **2004**, *25* (3), 129−131.
(15) Yang, Y.; Zhang, Y. H.; Shen, W. Z.; Liu, H. C. Semiconductor Infrared Up-Conversion Devices. *Prog. Quantum Electron.* **2011**, *35* (4), 77−108.
(16) Fu, C.; Mu, G.; Weng, K.; Tang, X. Advances in Organic Upconversion Devices. *Photonics* **2024**, *11* (9), 808.
(17) Bai, P.; Zhang, Y.; Wang, T.; Fu, Z.; Shao, D.; Li, Z.; Wan, W.; Li, H.; Cao, J.; Guo, X.; et al. Broadband THz to NIR Up-Converter for Photon-Type THz Imaging. *Nat. Commun.* **2019**, *10* (1), 3513.
(18) Lezhneva, G. M.; Melkadze, R. G.; Khvedelidze, L. V. GaAs Pixel-Detector Technology for X-Ray Medical Imaging: A Review. *Russ. Microelectron.* **2005**, *34* (4), 229−241.
(19) Becker, J.; Tate, M. W.; Shanks, K. S.; Philipp, H. T.; Weiss, J. T.; Purohit, P.; Chamberlain, D.; Gruner, S. M. Characterization of Chromium Compensated GaAs as an X-Ray Sensor Material for Charge-Integrating Pixel Array Detectors. *J. Instrum.* **2018**, *13* (1), P01007.
(20) Yanagida, T.; Kato, T.; Nakauchi, D.; Kawaguchi, N. Fundamental Aspects, Recent Progress and Future Prospects of Inorganic Scintillators. *Jpn. J. Appl. Phys.* **2023**, *62* (1), 010508.
(21) Yanagida, T. Inorganic Scintillating Materials and Scintillation Detectors. *Proc. Jpn. Acad. Ser. B* **2018**, *94* (2), 75−97.
(22) Ban, D.; Luo, H.; Liu, H. C.; Wasilewski, Z. R.; SpringThorpe, A. J.; Glew, R.; Buchanan, M. Optimized GaAs/AlGaAs Light-Emitting Diodes and High Efficiency Wafer-Fused Optical up-Conversion Devices. *J. Appl. Phys.* **2004**, *96* (9), 5243−5248.
(23) Bai, P.; Zhang, Y.; Wang, T.; Shi, Z.; Bai, X.; Zhou, C.; Xie, Y.; Du, L.; Pu, M.; Fu, Z.; Cao, J.; Guo, X.; Shen, W. Cryogenic Characteristics of GaAs-Based near-Infrared Light Emitting Diodes. *Semicond. Sci. Technol.* **2020**, *35* (3), 035021.
(24) Veale, M. C.; Bell, S. J.; Duarte, D. D.; French, M. J.; Hart, M.; Schneider, A.; Seller, P.; Wilson, M. D.; Kachkanov, V.; Lozinskaya, A. D.; Novikov, V. A.; Tolbanov, O. P.; Tyazhev, A.; Zarubin, A. N. Investigating the Suitability of GaAs: Cr Material for High Flux X-Ray Imaging. *J. Instrum.* **2014**, *9* (12), C12047−C12047.
(25) Ly Anh, T.; Perd'ochová, A.; Nečas, V.; Pavlicová, V. Radiation Resistance Study of Semi-Insulating GaAs-Based Radiation Detectors to Extremely High Gamma Doses. *Nucl. Phys. B, Proc. Suppl.* **2006**, *150*, 402−406.
(26) Khanna, R.; Han, S. Y.; Pearton, S. J.; Schoenfeld, D.; Schoenfeld, W. V.; Ren, F. High Dose Co-60 Gamma Irradiation of InGaN Quantum Well Light-Emitting Diodes. *Appl. Phys. Lett.* **2005**, *87* (21), 212107.
(27) Ban, D.; Luo, H.; Liu, H. C.; Wasilewski, Z. R.; Buchanan, M. Pixelless 1.5-μm up-Conversion Imaging Device Fabricated by Wafer Fusion. *IEEE Photonics Technol. Lett.* **2005**, *17* (7), 1477−1479.
(28) Nagarkar, V. V.; Gupta, T. K.; Miller, S. R.; Klugerman, Y.; Squillante, M. R.; Entine, G. Structured CsI(Tl) Scintillators for X-Ray Imaging Applications. *IEEE Trans. Nucl. Sci.* **1998**, *45* (3), 492−496.
(29) Collinson, A. J. L.; Hill, R. The Fluorescent Response of NaI(Tl) and CsI(Tl) to X Rays and γ Rays. *Proc. Phys. Soc.* **1963**, *81* (5), 883.
(30) Moszynski, M.; Balcerzyk, M.; Czarnacki, W.; Kapusta, M.; Klamra, W.; Syntfeld, A.; Szawlowski, M. Intrinsic Energy Resolution and Light Yield Nonproportionality of BGO. *IEEE Trans. Nucl. Sci.* **2004**, *51* (3), 1074−1079.
(31) Mao, R.; Zhang, L.; Zhu, R.-Y. Emission Spectra of LSO and LYSO Crystals Excited by UV Light, X-Ray and γ-Ray. *IEEE Trans. Nucl. Sci.* **2008**, *55* (3), 1759−1766.
(32) Li, G.; Wang, W.; Yang, W.; Lin, Y.; Wang, H.; Lin, Z.; Zhou, S. GaN-Based Light-Emitting Diodes on Various Substrates: A Critical Review. *Rep. Prog. Phys.* **2016**, *79* (5), 056501.
(33) Kneissl, M.; Seong, T.-Y.; Han, J.; Amano, H. The Emergence and Prospects of Deep-Ultraviolet Light-Emitting Diode Technologies. *Nat. Photonics* **2019**, *13* (4), 233−244.
(34) Hany, R.; Cremona, M.; Strassel, K. Recent Advances with Optical Upconverters Made from All-Organic and Hybrid Materials. *Sci. Technol. Adv. Mater.* **2019**, *20* (1), 497−510.
(35) Zhou, W.; Shang, Y.; García de Arquer, F. P.; Xu, K.; Wang, R.; Luo, S.; Xiao, X.; Zhou, X.; Huang, R.; Sargent, E. H.; Ning, Z. Solution-Processed Upconversion Photodetectors Based on Quantum Dots. *Nat. Electron.* **2020**, *3* (5), 251−258.
(36) Woo, J. Y.; Park, M.-H.; Jeong, S.-H.; Kim, Y.-H.; Kim, B.; Lee, T.-W.; Han, T.-H. Advances in Solution-Processed OLEDs and Their Prospects for Use in Displays. *Adv. Mater.* **2023**, *35* (43), 2207454.
(37) Yu, Q.; Wang, F.; Yuan, X.; Liu, Y.; Gan, L.; Xu, G.; Shen, W.; Chen, L.; Zhang, Y. An Alternative Application of GaAs-Based Light-Emitting Diodes: X-Ray Detection and Imaging. *arXiv*, **2025**.

https://doi.org/10.1021/acsphotonics.5c01458
ACS Photonics 2025, 12, 6028−6036